JOURNAL OF Materials CHEMISTRY

EPR evidence on short-range Co/Mn order in $LiCoMnO_4$ spinels

Radostina K. Stoyanova, Ekaterina N. Zhecheva* and Mila Y. Gorova

Institute of General and Inorganic Chemistry, Bulgarian Academy of Sciences, 1113 Sofia, Bulgaria. E-mail: zhecheva@svr.igic.bas.bg

Received 11th November 1999, Accepted 3rd March 2000
Published on the Web 11th May 2000

EPR of Mn^{4+} has been used to specify the electronic structure and cation distribution in $LiCoMnO_4$ compositions that belong to high-potential electrode materials. To prepare single phase $LiCoMnO_4$, two synthesis techniques have been adopted: solid state reactions and a lactate precursor method. EPR of Mn^{4+} shows that diamagnetic Co^{3+} (low-spin configuration, $S=0$) and paramagnetic Mn^{4+} ($S=3/2$) account for the electronic structure of $LiCoMnO_4$. Analysis of the EPR line width in terms of dipole–dipole and exchange interactions allows one to estimate the mean number of paramagnetic neighbours of Mn^{4+}. It has been demonstrated that the Co^{3+}/Mn^{4+} distribution in 16d spinel sites is sensitive towards the cooling rates. For the high-temperature $LiCoMnO_4$ phase obtained by air quenching from 750 °C, three paramagnetic Mn^{4+} and three diamagnetic Co^{3+} give rise to the local coordination of Mn^{4+}, indicating a random Co/Mn distribution. For the low-temperature $LiCoMnO_4$ phases obtained by air quenching from 600 °C and by slow-cooling from 750 to 25 °C, the mean paramagnetic number of Mn^{4+} decreases from 3 to 2, which is interpreted in the framework of short-range Co^{3+}/Mn^{4+} ordering. The Co^{3+}/Mn^{4+} octahedral ordering process is developed within a small-scale range (approximately up to a distance of the third metal shell) and does not affect the cubic spinel symmetry of $LiCoMnO_4$.

1 Introduction

Extensive studies have been devoted to the electrochemistry of $Li_{1+x}Mn_{2-x}O_4$ spinels in order to improve the cycle stability of these materials when used as cathodes in rechargeable lithium ion cells.[1–3] It has been found that, in the 3.5–4.5 V potential window, substitution of Co for Mn in $LiMn_2O_4$ leads to a decrease in the initial capacity and to a diminishing of the cycle fade.[4–11] Significant changes in the crystal structure and electrochemical properties of $LiMnO_2$ have been established when Co is substituted for Mn.[12–14] It has been found that the crystal structure of $LiCo_yMn_{1-y}O_2$ solid solutions depends on both the Co/Mn ratio and the synthesis conditions. At 800 °C, replacement of 20% Mn by Co leads to the formation of $LiCo_yMn_{1-y}O_2$ with a tetragonal spinel structure (s.g. $I4_1/amd$).[12] A further increases in the Co amount, $0.2<y<0.7$, causes a random distribution of Li, Co and Mn within the framework of the rock-salt type structure ($Fm3m$).[12] By a solution-based route coupled with ion-exchange at 150 °C, $LiCo_yMn_{1-y}O_2$, $0\leqslant y<0.5$, with a layered crystal structure can be obtained.[13,14] When this material is used as a cathode in lithium ion cells, a progressive conversion of the layered structure to the spinel one is observed on cycling.[14] Irrespective of the crystal structure type, $LiCo_yMn_{1-y}O_2$ solid solutions with $y<0.2$ exhibit a good cycle stability.[12–14] In an attempt to find new cathode materials with a working potential higher than 4.5 V, $Li[Co_{0.5}Mn_{1.5}]O_4$ and $LiCoMnO_4$ spinels have been recently reported.[11,15,16] In this connection, lithium–cobalt–manganese oxides will be of future interest as electrode materials in rechargeable lithium batteries.

$LiCoMnO_4$ is a normal spinel in which Li occupies tetrahedral 8a sites and Co/Mn are in octahedral 16d sites.[16–18] The charge distribution as determined by electron energy loss spectroscopy corresponds to $LiCo^{3+}Mn^{4+}O_4$, where Co^{3+} substitutes for Mn^{3+} in the normal $LiMn_2O_4$ spinel.[18] The similar atomic scattering factors of Co and Mn do not permit one to specify how these cations are distributed over 16d spinel sites. The possible Co/Mn ordering in 16d spinel sites will be of importance with a view to controlling the electrochemical properties of $LiCoMnO_4$ spinels. For example, there are data on the 1 : 3 cation ordering between M^{2+} (Mg, Co, Ni and Cu) and Mn^{4+} for $Li[M^{2+}_{1/2}Mn^{4+}_{3/2}]O_4$ spinels even in the case when no superstructure reflections are found after annealing because of a too small difference in the scattering power for X-rays between M^{2+} and Mn^{4+}.[19–21] In an attempt to investigate more carefully the electronic structure of pure $LiMn_2O_4$, a partial charge ordering below room temperature has been reported.[22–24] Two crystal structure types have been proposed for low-temperature $LiMn_2O_4$: a tetragonal variant of the Fdm spinel structure and a large orthorhombic cell.[22–24]

The availability of diamagnetic and paramagnetic ions (Co^{3+} and Mn^{4+}) in 16d positions provides an opportunity to use EPR of Mn^{4+} for a detailed study of the local coordination of these ions. Recently, we have demonstrated the power of the EPR of Mn^{4+} as an experimental tool to assess the local environment of Mn^{4+} in Mn^{4+}-rich $Li[Li_{1/3}Mn_{5/3}]O_4$ and stoichiometric $LiMn_2O_4$ spinels.[25,26]

In this article we provide EPR evidence on short-range Co/Mn order in the $LiCoMnO_4$ composition. Furthermore, we demonstrate the effect of the synthesis conditions on the Co/Mn ordering.

2 Experimental

2.1. Preparation of lithium–cobalt–manganese precursors

To prepare single phase $LiCoMnO_4$, we have used two synthesis routes. The first one includes a solid state reaction between mixed Co–Mn oxides and Li_2CO_3 and the second comprises thermal decomposition of the Li–Co–Mn lactate precursors.

Mixed Co–Mn oxides were obtained at 450 °C by thermal decomposition of co-precipitated Co–Mn carbonates at pH ≅ 7. The solid residue thus obtained was mixed intimately with an appropriate amount of Li_2CO_3 in a Fritsch planetary mill. This mixture was initially fired at 450 °C for 48 hours, then ground again, heated finally at 750 °C for 48 hours and cooled slowly to room temperature (about 1 °C min^{-1}). For sake of convenience, this sample will be denoted as ssr-750-sc.

Homogeneous LiCoMn lactates were prepared by freeze-drying of the corresponding solutions. Lithium–cobalt–manganese complexes with lactic acid were obtained by dissolution of Li_2CO_3, $CoCO_3$ and $MnCO_3$ in aqueous solutions of lactic acid (0.05 M). The ratio between the components was Li : Co : Mn : lactic acid = 1 : 1 : 1 : 6. Heating at 60 °C in an argon atmosphere proceeded to the formation of a clear solution, which was concentrated to 0.1 M (Co + Mn). Under these conditions, a stable solution with pH ≅ 4.5 was obtained. After complexation, the solutions were cooled down to room temperature, then frozen instantly with liquid nitrogen and dried in vacuum (20–30 mbar) at −20 °C in an Alpha-Crist Freeze-Dryer. Thermal decomposition of lactates in air at 450 °C yielded single phase $LiCoMnO_4$. To improve the crystallinity, the spinel was additionally annealed at 750 °C for 24 hours, two regimes being used for cooling to room temperature: (i) slow cooling with a rate of 1 °C min^{-1} and (ii) quenching by pouring out the powder between two metal plates. In some cases after annealing at 750 °C, the samples were cooled slowly to 600 °C, kept at this temperature for 10 hours and then quenched to room temperature. The slow-cooled, metal-quenched from 750 °C and 600 °C samples will be, further on, denoted by lac-750-sc, lac-750-mq and lac-750-600-mq, respectively.

2.2 Sample characterisation

The lithium content in the samples was determined by atomic absorption analysis. The total content of manganese and cobalt was established complexometrically and by atomic absorption analysis. The mean oxidation state of manganese and cobalt ions was established permanganometrically after dissolution of the powdered sample in a mixture of $VOSO_4$ and H_2SO_4 by titrating the excess of V^{4+} in the solution.[27]

The X-ray phase analysis was made by a Philips diffractometer with CuKα radiation. Unit cell parameters were obtained from least-square fitting of all peak positions. The infrared spectra were recorded on a Specord-75 (ex-GDR) spectrometer in KBr pellets. The magnetic susceptibility was determined by the Faraday method at 100–600 K.

The EPR spectra were recorded as a first derivative of the absorption signal of an ERS-220/Q (ex-GDR) spectrometer within the temperature range of 90–400 K. The *g* factors were determined with respect to a Mn^{2+}/ZnS standard. The signal intensity was established by double integration of the experimental EPR spectrum.

3 Results and discussion

3.1 Crystallochemistry of $LiCoMnO_4$

The two synthesis techniques described above allow the preparation of single phase $LiCoMnO_4$ with a cubic spinel structure, the lattice parameter being dependent on the synthesis conditions (Table 1). The lactate precursor method yields a $LiCoMnO_4$ spinel composition with a smaller lattice parameter, but the quenching of the spinels causes a drastic enlargement of the lattice dimensions. Contrary to the observed variation in lattice dimensions, the average oxidation state of Co/Mn only slightly depends on the cooling rates and is close to the theoretical one: 3.50 ± 0.01, 3.45 ± 0.01 and 3.48 ± 0.01 for slow cooled, quenched from 750 °C and quenched from 650 °C samples, respectively. This result reveals a sensitivity of the cation distribution towards the synthesis conditions.

Assuming a random Co/Mn distribution in 16d spinel sites, the unit cell parameter of $LiCoMnO_4$ solid solutions will be the averaged sum of the lattice parameters of the two end spinel compositions, $LiMn_2O_4$[28] and $LiCo_2O_4$:[29] $a = (8.24 + 7.99)/2 = 8.115$ Å. As one can see in Table 1, the calculated lattice parameter does not match either the lattice parameters experimentally obtained by us or the lattice parameters reported in literature.[9,16] The observed negative deviation implies a non-statistical distribution of Co/Mn, *i.e.* Co–Mn interactions are stronger that the Mn–Mn and Co–Co interactions, respectively. The supposed Co/Mn ordering will be developed at a small-scale range, so that the cubic spinel symmetry remains unchanged.

IR studies offer further information on the possible short-range order phenomena in $LiCoMnO_4$ compositions (Fig. 1). Two typical spinel bands at 520 and 630 cm^{-1} are clearly resolved in the IR spectra of all the samples investigated. The superimposed weak fine structure to the two spinel bands is consistent with the supposed Co/Mn short-range order model. The fine structure fades away for the quenched composition characterized by the higher lattice parameter. This means that the Co/Mn ordering mainly depends on the annealing temperature.

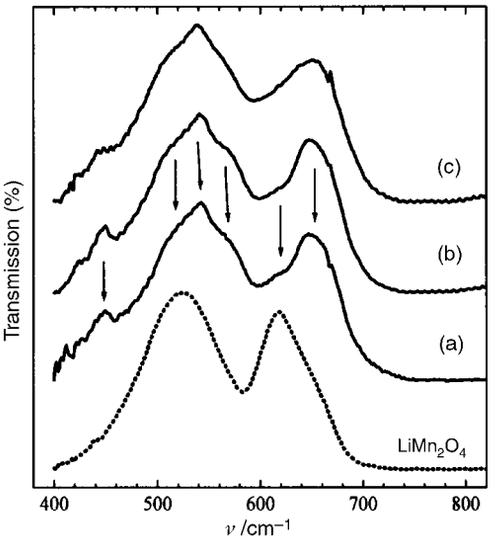

Fig. 1 IR spectra of $LiCoMnO_4$ obtained by a lactate precursor method: (a) lac-750-sc; (b) lac-750-600-mq and (c) lac-750-mq. For the sake of comparison, the IR spectrum of $LiMn_2O_4$ cooled slowly from 750 °C is also given.

Table 1 Unit cell parameters, *a*, metal–metal distance, r_{M-M}, temperature independent EPR line width, $\Delta H_{pp}{}^{\circ}$, Weiss constant, Θ, and mean number of paramagnetic ions, *z*, for $LiCoMnO_4$ obtained by solid state reactions and from lactate precursors

Sample	$a \pm 0.0004$/Å	r_{M-M}/Å	$\Delta H_{pp}{}^{\circ} \pm 0.3$/mT	$\Theta \pm 3$/K	$z \pm 0.3$
ssr-750-sc	8.0598	2.849	23.0	−30	2.3
lac-750-sc	8.0488	2.846	23.5	−28	2.3
lac-750-mq	8.0912	2.861	77.0	−13	3.2
lac-750-600-mq	8.0572	2.849	34.5	−19	2.4
Li_2MnO_3-ssr[25,37,38]	—	2.85	21.3	−44	3
ssr-750–600-quenched[16]	8.0519				
ssr-750-2 °C min^{-1} cooled[9]	8.097				

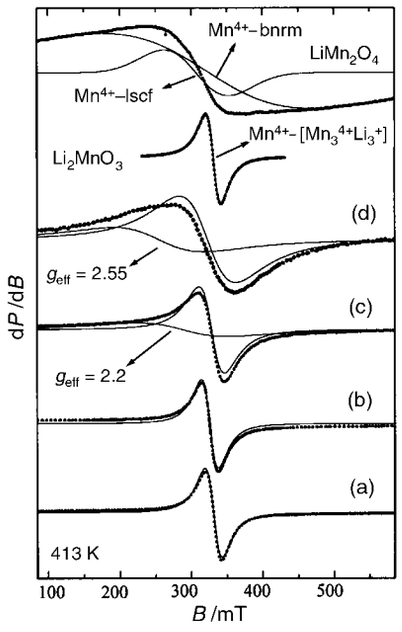

Fig. 2 EPR spectra at 413 K of $LiCoMnO_4$ obtained by a solid state reaction, ssr-750-sc (a), and by a lactate precursor method: (b) lac-750-sc; (c) lac-750-600-mq and (d) lac-750-mq. For sake of comparison, the EPR spectra of Li_2MnO_3 and $LiMn_2O_4$ are also given. Mn^{4+}-bnrm, Mn^{4+}-lscf and Mn^{4+}-[$Li^{+}{}_3Mn^{4+}{}_3$] denote EPR signals corresponding to Mn^{4+} in a bottle-neck regime, to Mn^{4+} in a low-symmetry crystal field and to Mn^{4+} in Li^{+}–Mn^{4+} environment.

3.2 EPR studies of Mn^{4+} in $LiCoMnO_4$

To get insight into the cation distribution in $LiCoMnO_4$, EPR of Mn^{4+} was undertaken. Fig. 2 gives the EPR spectra of $LiCoMnO_4$ compositions. The narrow line with Lorentzian shape and $g=2.002$ dominates in the EPR spectra of all the samples investigated (Fig. 2). The line width is narrowed as the recording temperature increases, reaching above 300 K a nearly constant value (Fig. 3). (The minimal value of the EPR line width will be denoted as a temperature independent line width, $\Delta H_{pp}{}^{\circ}$—Table 1.) A drastic increase in $\Delta H_{pp}{}^{\circ}$ is observed when $LiCoMnO_4$ is quenched from 750 °C. The intensity of the narrow Lorentzian line varies with the recording temperature, so that the Curie–Weiss law is obeyed. The experimentally obtained Weiss constants as well as the metal–metal distances (calculated from the unit cell parameters) are given in Table 1.

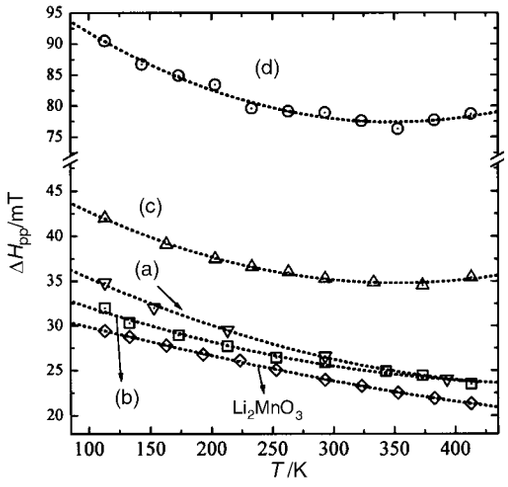

Fig. 3 Temperature variation in the EPR line width for $LiCoMnO_4$ obtained by a solid state reaction, ssr-750-sc (a), and by a lactate precursor method: (b) lac-750-sc; (c) lac-750-600-mq and (d) lac-750-mq. For the sake of comparison, the temperature dependence of the EPR line width for Li_2MnO_3 is also given.

As one can see in Table 1, there is a correlation between the temperature independent line width, the Weiss constant and the metal–metal distance: when the metal–metal distance decreases, the Weiss constant gains a higher value and the temperature independent line width is reduced.

In the low-magnetic field region of the EPR spectra of $LiCoMnO_4$ samples quenched from 750 and 600 °C, a broad line with a Lorentzian shape appears as a shoulder on the intense narrow Lorentzian with $g=2.002$ (Fig. 2). The effective g-factor and the intensity of this broad signal depend on the synthesis conditions. The effective g-value decreases from 2.55 to 2.20 for $LiCoMnO_4$ quenched from 750 and 600 °C, respectively (Fig. 2). In the same order, the signal intensity decreases (Fig. 2).

To assign the observed EPR signals, Fig. 2 compares the EPR spectra of $LiCoMnO_4$ with the spectra of two types of lithium manganese oxides: one containing Mn^{4+} only (layered Li_2MnO_3) and the other characterized by Mn^{3+} and Mn^{4+} in equal amounts (spinel $Li[Mn^{3+}Mn^{4+}]O_4$). In accordance with previous studies,[25,30] the EPR spectrum of Li_2MnO_3 consists of a narrow Lorentzian line with $g=1.995$ due to the magnetic coupled Mn^{4+} in ($LiMn_2$) layers (Fig. 2). The antiferromagnetic interactions between Mn^{4+} ions in Li_2MnO_3 produce broadening of the EPR line width as the recording temperature decreases (Fig. 3). At 410 K, the EPR line width becomes nearly constant. The temperature dependence of the signal intensity obeys the Curie–Weiss law, the Weiss constant being −44 K. The appearance of paramagnetic Mn^{3+} in the local environment of Mn^{4+} causes a drastic change in the EPR spectra of Mn^{4+}. In this case, the direct relaxation of Mn^{4+} to the lattice is not effective enough to disturb the collective motion of the total magnetic moment of the Mn^{3+} and Mn^{4+} spin systems.[26] As a result, the relaxation mechanism, referred to as a bottle-neck relaxation mechanism, governs the temperature-induced variations in line width and in signal intensity. In addition, the EPR spectrum of $LiMn_2O_4$ shows a low-intensity signal with $g>2.0$, which has been attributed to complex associates of defects including several Mn^{4+} in a low-symmetry crystal field and oxygen vacancies.[26]

Close inspection of the EPR spectra of $LiCoMnO_4$, Li_2MnO_3 and $LiMn_2O_4$ shows that the characteristic features of the intense narrow Lorentzian line bear resemblance to those of a signal due to antiferromagnetically coupled Mn^{4+} in Li_2MnO_3. This means that antiferromagnetically interacting Mn^{4+} account for the EPR profile of $LiCoMnO_4$ spinels. Indirectly, the EPR results prove that the charge distribution in $LiCoMnO_4$ corresponds to diamagnetic Co^{3+} and paramagnetic Mn^{4+}. Moreover, the normalized intensity of the EPR signal for $LiCoMnO_4$ is close to the normalized intensity of antiferromagnetically coupled Mn^{4+} in Li_2MnO_3: $\{I_{mol}(T-\Theta)\}^{1/2}=1.0$, 0.92 and 0.78 for Li_2MnO_3, metal quenched $LiCoMnO_4$ and slowly cooled $LiCoMnO_4$.

The contribution of diamagnetic Co^{3+} and paramagnetic Mn^{4+} to the electronic structure of $LiCoMnO_4$ was further proven by magnetic susceptibility measurements. The Curie constant determined for slow-cooled $LiCoMnO_4$ is 1.92 ± 0.02, which is typical for the spin-only value for Mn^{4+}, $C_{Curie}=1.90$. In addition, the Weiss constant is $-(38\pm4)$ K, which matches satisfactorily the Weiss constant determined by EPR: $-(28\pm3)$ K.

Considering the effective g-factors, the origin of the low-intensity signal in the EPR spectra of the quenched from 750 °C and 650° samples is not clear. However, in comparison with the EPR spectrum of $LiMn_2O_4$, the low-intensity broad signal in the EPR spectrum of $LiCoMnO_4$ can be tentatively assigned to complex [Mn–Co] clusters near oxygen defects (Fig. 2). Since the amount of these clusters increases for quenched $LiCoMnO_4$ samples that are slightly oxygen deficient it seems that these [Mn–Co] clusters occupy mainly surface sites, which are in close contact with the oxygen from the atmosphere. The

formation of [Co–Mn] clusters is a not unexpected result if we consider the defect structure of cubic $LiMn_2O_4$ with a slight oxygen deficiency.[31] Using data from neutron diffraction, an oxygen vacancy cluster model, where four MnO_4 species are connected by a common corner situated at 8b interstitial oxygen ions, was recently proposed for $LiMn_2O_4$.[31]

3.3 Short-range Co^{3+}/Mn^{4+} octahedral ordering in $LiCoMnO_4$

For the purpose of studying the Co/Mn cation distribution as a function of the synthesis conditions, analyses of the EPR line width of antiferromagnetically coupled Mn^{4+} have been carried out for $LiCoMnO_4$ prepared with various cooling rates. According to the EPR theory for magnetically concentrated systems, the dipole–dipole and exchange interactions give rise to the EPR line width as compared to the EPR line of isolated spins. Depending on the spin concentration and the distance between the spins, dipole–dipole interactions are superimposed on the Zeeman's interactions, thus leading to an increase in line width. Contrary to the dipole–dipole interactions, the exchange interactions average the local magnetic field around the paramagnetic species, as a result of which the line width decreases. Following the method of moments,[32–34] the mutual contribution of the dipole–dipole, $M_{dd}{}^2$, and the exchange interactions, H_e, to the line width is expressed by

$$\Delta H_{pp} = \text{const}\ \frac{M_{dd}{}^2}{H_e} = \text{const}\ \frac{g^2 S(S+1) \sum_{i,k} (1-3\ \cos^2\ \Theta_{ik})/r_{i,k}{}^6}{\sqrt{\frac{8}{3} S(S+1) z J}} \quad (1)$$

where z, $r_{i,k}$ and $\Theta_{i,k}$ denote the number of paramagnetic nearest neighbours particles, the distance between them and the angle of the radius vector between two spins with the magnetic field, respectively; J corresponds to the strength of exchange interactions. In the case of polycrystalline samples, the average angular term is 4/5. For a spinel lattice, the first, second and third metal neighbours will contribute 95.0%, 3.5% and 1.5%, respectively, to the line width. As a first approximation, this allows restriction of the dipole–dipole contribution up to the first neighbours. In order to rationalize this formula, the exchange term can be replaced by the experimentally accessible Weiss constant, $\Theta = 2/3 S(S+1) zJ/k$.

$$\Delta H_{pp} = \text{const}\ g^2 \beta^2\ \frac{\{S+1)\}^{3/2} z^{3/2}}{r^6 \Theta} \quad (2)$$

The strength of the antiferromagnetic interactions between Mn^{4+} (estimated from the Weiss constant) increases as the metal–metal distance decreases (Table 1). This result conforms very well to the data on Mn^{4+} magnetic interactions developed in λ-MnO_2 and $Li[Li_{1/3}Mn_{5/3}]O_4$ spinels. With increasing metal–metal distance from 2.84 to 2.88 Å, the antiferromagnetic interactions drop in magnitude and ferromagnetic interactions take place.[35,36] By a comparative analysis of the EPR line width for Mn^{4+} in $LiCoMnO_4$ and Li_2MnO_3, it is possible to eliminate the unknown quantity in the above formula.

$$z = \left\{ z^{3/2}_{Li_2MnO_3}\ \frac{(\Delta H_{pp}\Theta)}{(H_{pp}\Theta)_{Li_2MnO_3}}\ \left(\frac{g_{Li_2MnO_3}}{g}\right)^2 \left(\frac{r_{Li_2MnO_3}}{r}\right)^{-6} \right\}^{2/3} \quad (3)$$

Since the crystal structure data and EPR parameters for Mn^{4+} in Li_2MnO_3 are well documented,[25,30,37,38] we are able to give a real estimation of the mean number of paramagnetic ions around Mn^{4+} in the $LiCoMnO_4$ composition (Table 1). For the sample quenched from 750 °C, the mean number of paramagnetic neighbours of Mn^{4+} is nearly 3, while for the slow-cooled sample and that quenched from 600 °C the mean number of Mn^{4+} tends to 2.

In the case of random Co/Mn distribution in 16d spinel sites, each Mn will have three diamagnetic Co^{3+} and three paramagnetic Mn^{4+} ions as first neighbours. This expected number of paramagnetic neighbours of Mn^{4+} is close to that observed for a $LiCoMnO_4$ sample quenched from 750 °C, which indicates a tendency to a random Co/Mn distribution. The negative deviation of the observed mean number of paramagnetic neighbours reveals a non-random Co/Mn distribution in $LiCoMnO_4$ cooled slowly from 750 °C and quenched from 600 °C.

Two types of 1 : 1 cation ordering in 16d spinel sites are known (Fig. 4). Both of them are similar with respect to the first metal shell: every ion's first neighbours are 4 "alien" and 2 "allied" ions. Second and third metal shells allow differentiation between the two types of 1 : 1 ordering (Table 2). Since the first metal neighbours have the major contribution to the EPR line width (95.0%), the two types of 1 : 1 ordering are not clearly distinguishable by analysis of the EPR line width. However, if we consider the contribution of the second and third metal shells to the EPR line width, the mean number of paramagnetic neighbours will be slightly higher than 2 (Table 2). This is what we observe for the mean number of paramagnetic neighbours in $LiCoMnO_4$ cooled slowly from 750 °C and quenched from 600 °C. For sake of comparison, Table 2 gives the number of the first, second and third neighbours of Mn^{4+} in a 1 : 3 octahedral ordering for $Li[M^{2+}{}_{1/2}Mn^{4+}{}_{3/2}]O_4$ spinels.[19–21]

4 Conclusions

EPR of Mn^{4+} shows that diamagnetic Co^{3+} (low-spin configuration) and paramagnetic Mn^{4+} account for the electronic structure of $LiCoMnO_4$. Analysis of the EPR line width allows estimation of the mean number of paramagnetic neighbours of Mn^{4+} in 16d spinel sites. For $LiCoMnO_4$ quenched from 750 °C, the mean number of Mn^{4+} is close to 3, while with decreasing cooling rate, the mean number of neighbouring Mn^{4+} decreases from 3 to 2. These results show that a random Co^{3+}/Mn^{4+} distribution is achieved for high-

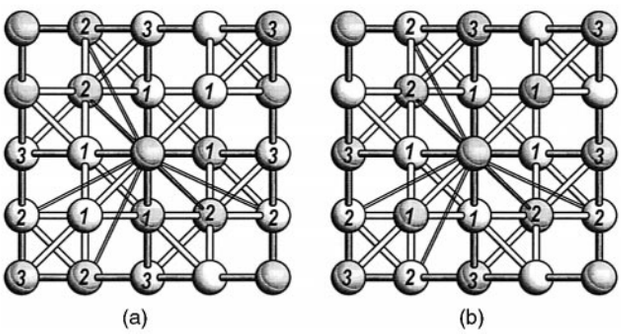

Fig. 4 Schematic presentation of 1 : 1 octahedral ordering: (a) α-type and (b) β-type. First, second and third neighbours are denoted.

Table 2 Coordination number, z, for the first, second and third metal shell and mean paramagnetic number, $\overline{z_{par}}$, for α-type and β-type 1 : 1 octahedral ordering, as well as for in 1 : 3 octahedral ordering

r_{M-M}/Å	z	α-type	β-type	1 : 3 order
r	6	2–4	2–4	4–2
$\sqrt{3}r$	6	4–2	2–4	4–2
$2r$	6	2–4	6–0	6–0
	$\overline{z_{par}}$ =	2.07	2.06	4.03

temperature phases obtained by air quenching from 750 °C, while a tendency for local Co^{3+}/Mn^{4+} ordering takes place for low-temperature phases obtained by air quenching from 600 °C and by slow cooling from 750 to 25 °C. The Co^{3+}/Mn^{4+} octahedral ordering occurs at a distance of the third metal shell and does not affect the cubic spinel symmetry of $LiCoMnO_4$.

Acknowledgements

Financial support from the National Science Fund of Bulgaria (Contract no. Ch810/1998) is gratefully acknowledged.

References

1 M. M. Thackeray, W. I. F. David, P. Bruce and J. B. Goodenough, *Mater. Res. Bull.*, 1983, **18**, 461.
2 R. Koksbang, J. Barker and M. Y. Saïdi, *Solid State Ionics*, 1996, **84**, 1.
3 M. Winter, J. O. Besenhard, M. E. Spahr and P. Novak, *Adv. Mater.*, 1998, **10**, 725.
4 R. Bittihn, R. Herr and D. Hoge, *J. Power Sources*, 1993, **43–44**, 223.
5 W. Baochen, X. Yongyao, F. Li and Z. Dongjiang, *J. Power Sources*, 1993, **43–44**, 539.
6 L. Guohua, H. Ikuta, T. Uchida and M. Wakihara, *J. Electrochem. Soc.*, 1996, **143**, 178.
7 G. Pistoia, A. Antonini, R. Rosati and C. Bellito, *J. Electroanal. Chem.*, 1996, **410**, 115.
8 L. Sanchez and J.-L. Tirado, *J. Electrochem. Soc.*, 1997, **144**, 1939.
9 P. Arora, B. N. Popov and R. E. White, *J. Electrochem. Soc.*, 1998, **145**, 807.
10 H. Hosoya, H. Ikuta and M. Wakihara, *Solid State Ionics*, 1998, **111**, 153.
11 H. Kawai, M. Nagata, H. Kageyama, H. Tukamoto and A. R. West, *Electrochim. Acta*, 1999, **45**, 315.
12 R. Stoyanova, E. Zhecheva and L. Zarkova, *Solid State Ionics*, 1994, **73**, 233.
13 A. R. Armstrong, R. Gitzendanner, A. D. Robertson and P. Bruce, *Chem. Commun.*, 1998, 1833.
14 A. R. Armstrong, A. D. Robertson, R. Gitzendanner and P. Bruce, *J. Solid State Chem.*, 1999, **145**, 549.
15 H. Kawai, M. Nagata, H. Tukamoto and A. R. West, *J. Mater. Chem.*, 1998, **8**, 837.
16 H. Kawai, M. Nagata, H. Tukamoto and A. R. West, *Electrochem. Solid-State Lett.*, 1998, **1**, 212.
17 G. Blasse, *Philips Res. Rep. Suppl.*, 1964, **3**, 121.
18 S. Suzuki, M. Tomita, S. Okada and H. Arai, *J. Phys. Chem. Solids*, 1996, **57**, 1851.
19 G. Blasé, *J. Inorg. Nucl. Chem.*, 1964, **26**, 1473.
20 J. Preudhomme, *C. R. Acad. Sci. (France)*, 1968, **C267**, 163.
21 D. Gryffroy and R. E. Vandenberghe, *J. Phys. Chem. Solids*, 1992, **53**, 777.
22 A. Yamada and M. Tanaka, *Mater. Res. Bull.*, 1995, **30**, 715.
23 A. S. Wills, N. P. Raju and J. E. Greedan, *Chem. Mater.*, 1999, **11**, 1510.
24 J. Rodriguez-Carvajal, G. Rousse, C. Masquelier and M. Hervieu, *Phys. Rev. Lett.*, 1998, **81**, 4660.
25 R. Stoyanova, M. Gorova and E. Zhecheva, *J. Phys. Chem. Solids*, 2000, **61**, 615.
26 R. Stoyanova, M. Gorova and E. Zhecheva, *J. Phys. Chem. Solids*, 2000, **61**, 609.
27 D. G. Wickham and E. R. Whipple, *Talanta*, 1963, **10**, 314.
28 D. G. Wickham and W. J. Croft, *J. Phys. Chem. Solids*, 1958, **7**, 351.
29 R. J. Gummow, D. C. Liles, M. M. Thackeray and W. I. F. David, *Mater. Res. Bull.*, 1993, **28**, 1177.
30 V. Massarotti, D. Capsoni, M. Bini and C. B. Azzoni, *J. Solid State Chem.*, 1997, **128**, 80.
31 R. Kanno, A. Kondo, M. Yonemura, R. Gover, Y. Kawamoto, M. Tabuchi, T. Kamiyama, F. Izumi, C. Masquelier and G. Rousse, *J. Power Sources*, 1999, **81–82**, 542.
32 J. H. Van Vleck, *Phys. Rev.*, 1948, **74**, 1168.
33 P. W. Anderson and P. R. Weiss, *Rev. Mod. Phys.*, 1953, **25**, 269.
34 T. Morya, *Prog. Theor. Phys. Kyoto*, 1956, **16**, 23.
35 J. E. Greedan, N. P. Raju, A. S. Wills, C. Morin and S. M. Shaw, *Chem. Mater.*, 1998, **10**, 3058.
36 C. Masquelier, M. Tabuchi, K. Ado, R. Kanno, Y. Kobayashi, Y. Maki, O. Nakamura and J. B. Goodenough, *J. Solid State Chem.*, 1996, **123**, 255.
37 P. Strobel and B. Lambert-Anderson, *J. Solid State Chem.*, 1988, **75**, 90.
38 A. Riou, Y. Lecere, Y. Gerault and Y. Cudennec, *Mater. Res. Bull.*, 1992, **27**, 269.